Published in IET Optoelectronics
Received on 29th October 2008
Revised on 3rd March 2009
doi: 10.1049/iet-opt.2008.0059

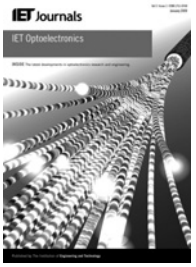

ISSN 1751-8768

Coded-orthogonal frequency division multiplexing in hybrid optical networks

I.B. Djordjevic

Department of Electrical and Computer Engineering, University of Arizona, Tucson, AZ 85721, USA
E-mail: ivan@ece.arizona.edu

Abstract: Future Internet should be able to support a wide range of services containing large amount of multimedia over different network types at a high speed. The future optical networks will therefore be hybrid, composed of different single-mode fibre (SMF), multi-mode fibre (MMF) and free-space optical (FSO) links. In these networks, novel modulation and coding techniques are needed that are capable of dealing with different channel impairments, be it in SMF, MMF or FSO links. The authors propose a coded-modulation scheme suitable for use in hybrid FSO – fibre-optics networks. The proposed scheme is based on polarisation-multiplexing and coded – orthogonal frequency division multiplexing (OFDM) with large girth quasi-cyclic low-density parity-check (LDPC) codes as channel codes. The proposed scheme is able to simultaneously deal with atmospheric turbulence, chromatic dispersion and polarisation mode dispersion (PMD). With a proper design for 16-quadrature amplitude modulation (QAM)-based polarisation-multiplexed coded-OFDM, the aggregate data rate of 100 Gb/s can be achieved for OFDM signal bandwidth of only 12.5 GHz, which represents a scheme compatible with 100 Gb/s per wavelength channel transmission and 100 Gb/s Ethernet.

1 Introduction

The transport capabilities of fibre-optic communication systems have increased tremendously, primarily because of advances in optical devices and technologies, and have enabled the Internet as we know it today with all its impacts on the modern society. In particular, dense wavelength division multiplexing (DWDM) became a viable, flexible and cost-effective transport technology [1–9]. Optical communication systems are developing rapidly because of the increased demands on transmission capacity. For example, the network operators are already considering 100 Gb/s per DWDM channel transmission [2]. The free-space optical (FSO) communication [10–12] is the technology that can address any connectivity needs in optical networks, be it in the core, edge or access. In metropolitan area networks (MANs), the FSO can be used to extend the existing MAN rings; in enterprise, the FSO can be used to enable local area network (LAN)-to-LAN connectivity and intercampus connectivity; and the FSO is an excellent candidate for the last-mile connectivity [11]. The future optical networks will allow the integration of fibre optics and FSO technologies, and will, therefore, have different portions of network being composed of fibre [either single-mode fibre (SMF) or multi-mode fibre (MMF)] and FSO sections. These hybrid optical networks might have a significant impact in both military and commercial applications, when pulling the ground fibre is expensive and takes a long time for deployment. Given the fact that hybrid optical networks will contain both FSO and fibre-optic sections, one has to study not only how to deal with atmospheric turbulence present in the FSO portion of the network, but also the influence of fibre non-linearities, PMD and chromatic dispersion in the fibre-optic portion of the network.

In this paper, we propose a coded-modulation scheme that is able to simultaneously deal with atmospheric turbulence, chromatic dispersion and polarisation-mode dispersion (PMD) in future hybrid optical networks. Moreover, the proposed scheme supports 100 Gb/s per DWDM channel transmission and 100 Gb/s Ethernet, while employing the mature 10 Gb/s fibre-optics technology. The proposed hybrid optical network scheme employs the orthogonal frequency division multiplexing (OFDM) as the multiplexing and modulation technique, and uses the

low-density parity-check (LDPC) codes as channel codes. With a proper design for 16 quadrature amplitude modulation (QAM)-based polarisation-multiplexed coded-OFDM, the aggregate data rate of 100 Gb/s can be achieved for the OFDM signal bandwidth of only 12.5 GHz, which represents a scheme suitable for 100 Gb/s Ethernet. Note that arbitrary forward error correction (FEC) scheme can be used in proposed hybrid optical network. However, the use of large girth LDPC codes [2] leads to the channel capacity achieving performance.

We consider two scenarios: (i) the FSO channel characteristics are known on the transmitter side and (ii) the FSO channel characteristics are not known on the transmitter side. In both scenarios, we assume that fibre-optic channel properties are known on the receiver side, obtained by pilot-aided channel estimation. Given the fact that transmitter and receiver nodes might be connected through several FSO and fibre-optic links, and that FSO link properties can vary significantly during the day, it is reasonable to assume that FSO link channel conditions are not known on the receiver side. In the presence of rain, snow and fog, we assume that an RF feedback channel is used to transmit the channel coefficients to the transmitter, which adapts the transmitted power and data rate according to the channel conditions.

The proposed scheme has many unique advantages: (i) demodulation, equalisation and decoding are jointly performed; (ii) it is able to operate in the presence of channel impairments over different optical links, be it in SMF, MMF or FSO, (iii) it has high-bandwidth efficiency (even 10 bits/s/Hz), (iv) it is compatible with future 100 Gb/s Ethernet technologies; and (v) the employed coded modulation provides excellent coding gains. We also describe about how to determine the symbol reliabilities in the presence of laser phase noise, and describe a particular channel inversion technique suitable for dealing with PMD effects.

The paper is organised as follows. In Section 2 we describe the proposed hybrid optical network and the corresponding coded-modulation scheme. In Section 3 we describe the channel model, whereas in Section 4 we describe the receiver architecture and transmission diversity principle. In Section 5 we report numerical results, and some important conclusions are given in Section 6.

2 Description of the proposed hybrid optical network

An example of a hybrid FSO – fibre-optic network is shown in Fig. 1*a*. This particular example includes inter-satellite links and connection to aircrafts. The fibre-optic portion of the network could be a part of already installed MAN or wide area network (WAN). The FSO network portion should be used whenever pulling the ground fibre is

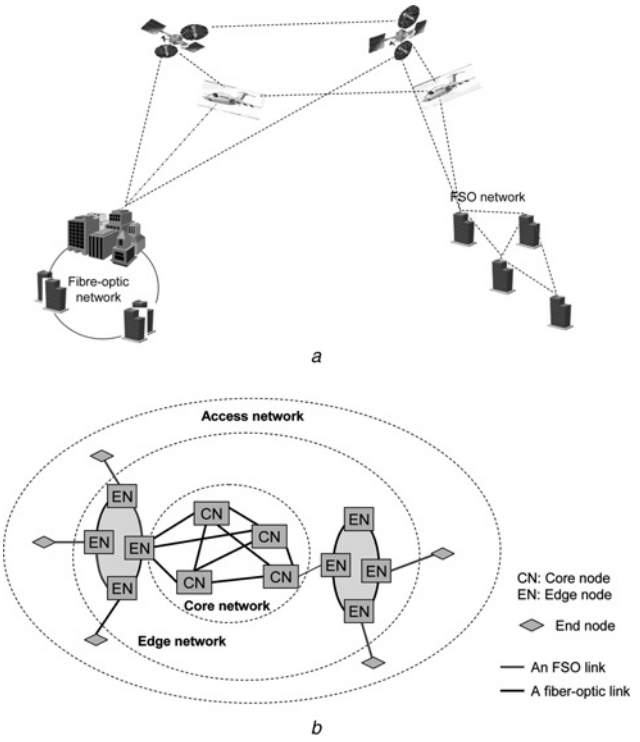

Figure 1 *Illustration of hybrid optical networking principle*
a A hybrid FSO – fibre-optic network example
b Hybrid optical networking architecture

expensive and/or takes too much time for deployment, such as urban and rural areas, where the optical fibre links are not installed. The corresponding hybrid optical networking architecture is shown in Fig. 1*b*. We can identify three ellipses representing the core network, the edge network and the access network. The FSO links can be used in both edge and access networks. The hybrid optical networks impose a big challenge to the engineers, because the novel signal processing techniques should be developed, which would be able to simultaneously deal atmospheric turbulence in FSO links, and with chromatic dispersion, PMD and fibre non-linearities in fibre-optic links. One such coded-modulation technique is described in the rest of this section. By using the retro-reflectors the FSO systems can be applied even when there is no line of sight between the transmitter and the receiver.

The proposed coded-modulation scheme employs the coded-OFDM scheme with coherent detection. Note that the coded-OFDM scheme with direct detection has already been proposed by the authors in [12], as a scheme that in combination with interleaving is able to operate under strong atmospheric turbulence. The use of coherent detection offers the potential of even 24 dB improvement over uncoded direct detection counterpart. One portion of improvement (10–13 dB) is comes from the fact that coherent detection can approach quantum-detection limit easier than direct detection. The second portion (about 11 dB) comes from the use of large-girth LDPC codes [1, 2]. Let us now describe the operation principle of

doi: 10.1049/iet-opt.2008.0059

coded-OFDM scheme with coherent detection employing both polarisations. Given the fact that the signal from Fig. 1 is going to be transmitted over the FSO links and over the fibre-optic links, we use a particular polarisation multiplexing capable of eliminating the influence of PMD. The transmitter and the receiver shown in Fig. 2, to be used in hybrid optical network from Fig. 1, are able to simultaneously deal with atmospheric turbulence, residual chromatic dispersion and PMD. The bit streams originating from m different information sources are encoded using different (n, k_i) LDPC codes of code rate $r_i = k_i/n$. k_i denotes the number of information bits of the ith $(i = 1, 2, \ldots, m)$ component LDPC code, and n denotes the codeword length, which is the same for all

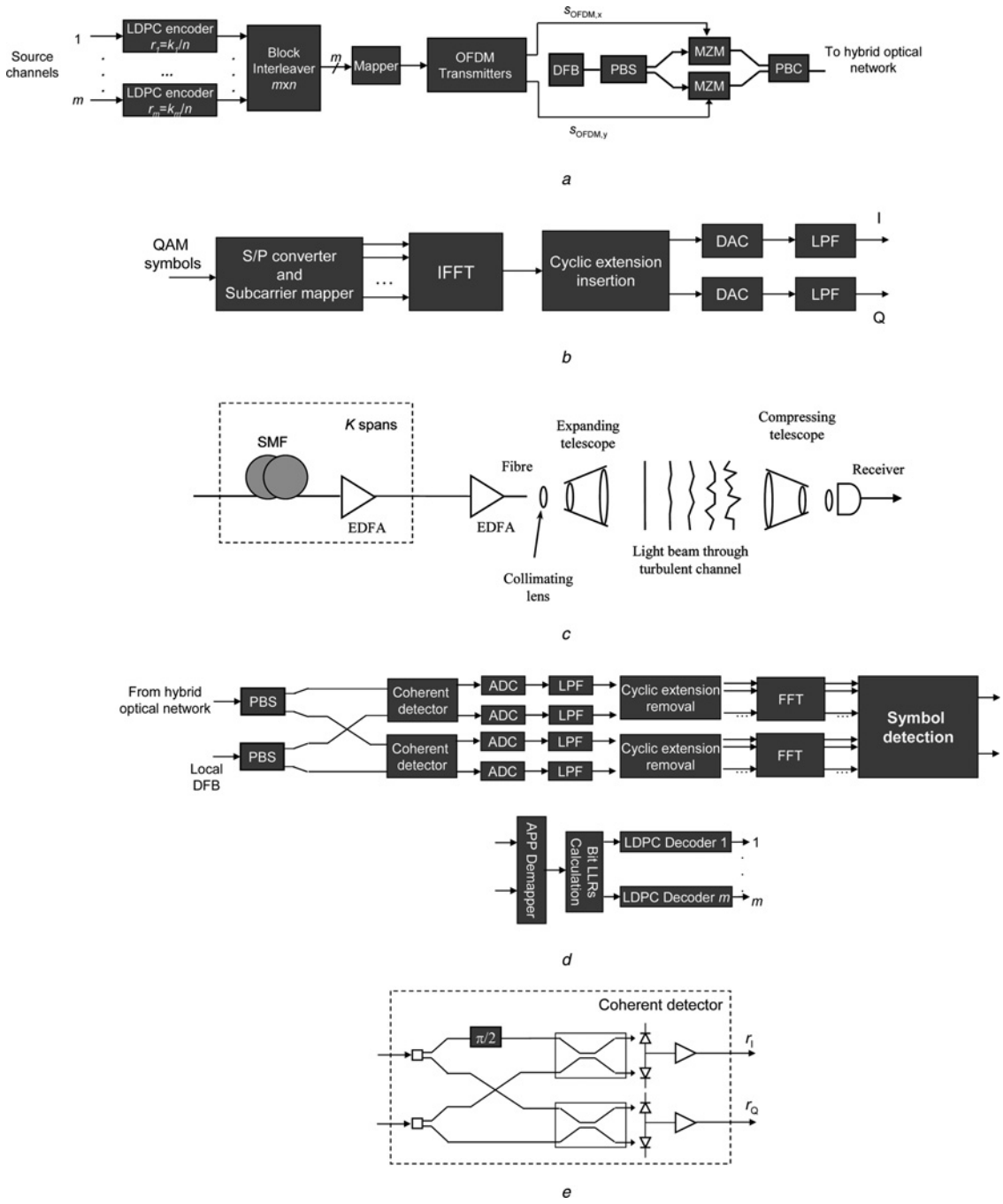

Figure 2 *Transmitter and receiver configurations for LDPC-coded OFDM hybrid optical system with polarisation multiplexing and coherent detection*

a Transmitter architecture
b OFDM transmitter architecture
c Hybrid optical link example
d Receiver architecture
e Coherent detector configuration. PBS/PBC

LDPC codes. The use of different LDPC codes allows us to optimally allocate the code rates. If all component LDPC codes are identical, then the corresponding scheme is commonly referred to as the bit-interleaved coded modulation (BICM). The outputs of m LDPC encoders are written row-wise into a block-interleaver block. The mapper accepts m bits at time instance i from the $(m \times n)$ interleaver column-wise and determines the corresponding M-ary ($M = 2^m$) signal constellation point ($\phi_{I,i}$, $\phi_{Q,i}$) in a two-dimensional (2D) constellation diagram such as M-ary phase-shift keying (PSK) or M-ary QAM. (The coordinates correspond to in-phase and quadrature components of M-ary 2D constellation.)

The OFDM symbol is generated as described below. N_{QAM} input QAM symbols are zero padded to obtain N_{FFT} input samples for inverse fast Fourier transform (IFFT) (the zeros are inserted in the middle rather than at the edges), and N_{G} non-zero samples are inserted to create the guard interval. For efficient chromatic dispersion and PMD compensation, the length of the cyclically extended guard interval should be longer than the total spread because of chromatic dispersion and maximum value of differential group delay (DGD). The cyclic extension is obtained by repeating the last $N_{\mathrm{G}}/2$ samples of the effective OFDM symbol part (N_{FFT} samples) as a prefix, and repeating the first $N_{\mathrm{G}}/2$ samples as a suffix. After D/A conversion (DAC), the OFDM signal is converted into the optical domain using the dual-drive Mach–Zehnder modulators (MZMs). Two dual-drive MZMs are needed, one for each polarisation. The outputs of MZMs are combined using the polarisation beam combiner (PBC). The same distributed feedback (DFB) laser is used as a CW source, with x- and y-polarisations being separated by a polarisation beam splitter (PBS).

The operations of all other blocks in the transmitter are similar to those we reported in [9, 12], and for more details on OFDM with coherent detection an interested reader is referred to an excellent tutorial paper by Shieh *et al.* [4].

The key idea of this proposal is to use the OFDM with a large number of subcarriers (in the order of thousands) so that the OFDM symbol duration becomes in order of μs, and by means of interleavers in the order of thousands overcome the atmospheric turbulence with temporal correlation in the order of 10 ms. For the OFDM scheme to be capable of simultaneously compensating for chromatic dispersion and PMD, in addition to the atmospheric turbulence, the cyclic extension guard interval should be longer than the total delay spread because of chromatic dispersion and DGD, as indicated above.

The OFDM is also an excellent candidate to be used for multi-user access [known as OFDM access (OFDMA)]. In OFDMA, subsets of subcarriers are assigned to individual users. OFDMA enables time and frequency domain resource partitioning. In time domain, it can accommodate for the burst traffic (packet data) and enables multi-user diversity. In frequency domain, it provides further granularity and channel-dependent scheduling. In OFDMA, different numbers of sub-carriers can be assigned to different users, in order to support differentiated quality of service (QoS). Each subset of sub-carriers can have different kinds of modulation formats, and can carry different types of data. The differentiated QoS can be achieved by employing the LDPC codes of different error correction capabilities. The OFDMA, therefore, represents an excellent interface between wireless/wireline and optical technologies.

Because for high-speed signals a longer sequence of bits is affected by the deep fade in the ms range due to atmospheric turbulence, we propose to employ the polarisation multiplexing and large QAM constellations in order to achieve the aggregate data rate of $R_{\mathrm{D}} = 100$ Gb/s, while keeping the OFDM signal bandwidth in the order of 10 GHz. For example, by using the polarisation-multiplexing and 16-QAM, we can achieve $R_{\mathrm{D}} = 100$ Gb/s for a OFDM signal bandwidth of 12.5 GHz, resulting in a bandwidth efficiency of 8 bits/s/Hz. Similarly, by using the polarisation multiplexing and 32-QAM we can achieve the same data rate ($R_{\mathrm{D}} = 100$ Gb/s) for a OFDM signal bandwidth of 10 GHz, with a bandwidth efficiency of 10 bits/s/Hz.

The receiver description requires certain knowledge of the channel. In what follows, we assume that fibre-optic channel characteristics are known on the receiver side, because the fibre-optics channel coefficients can easily be determined by pilot-aided channel estimation. On the other hand, the hybrid optical network may contain different FSO and fibre-optic sections, while the channel characteristics of the FSO link can change rapidly even during the day, it is reasonable to assume that FSO channel characteristics are not known on the receiver side. The FSO transmitter can use a retro-reflector and a training sequence to sense the FSO channel. We will further describe two concepts: (i) the transmitter does not have any knowledge about the FSO link and (ii) the transmitter knows the FSO link properties. When the transmitter knows the FSO link properties, we can employ the transmitter diversity concept. Before resuming our description of the coded-OFDM receiver, in the next section we provide more details about FSO and fibre-optic channel models.

3 Description of the channel model

A commonly used turbulence model assumes that the variations of the medium can be understood as individual cells of air or eddies of different diameters and refractive indices. In the context of geometrical optics, these eddies may be observed as lenses that randomly refract the optical wave front, generating a distorted intensity profile at the

doi: 10.1049/iet-opt.2008.0059

receiver of a communication system. The amplitude and phase fluctuations, also known as scintillation, represent the most important factors that limit the performance of an atmospheric FSO communication link. The most widely accepted theory of turbulence is given by Kolmogorov [10]. This theory assumes that kinetic energy from large turbulent eddies, characterised by the parameter known as outer scale L_0, is transferred without loss to the eddies of decreasing size down to sizes of a few millimetres characterised by the inner scale parameter l_0. The inner scale represents the cell size at which energy is dissipated by viscosity. The refractive index varies randomly across different turbulent eddies and causes phase and amplitude variations to the wave front. To account for the strength of the turbulence, we use the unitless Rytov variance, given by [10]

$$\sigma_{\mathrm{R}}^2 = 1.23\ C_n^2\ k^{7/6} L^{11/6} \tag{1}$$

where $k = 2\pi/\lambda$ is the wave number, λ is the wavelength, L is the propagation distance and C_n^2 denotes the refractive index structure parameter, which is constant for horizontal paths. Weak fluctuations are associated with $\sigma_{\mathrm{R}}^2 < 1$, the moderate with $\sigma_{\mathrm{R}}^2 \simeq 1$, the strong with $\sigma_{\mathrm{R}}^2 > 1$ and the saturation regime is defined by $\sigma_{\mathrm{R}}^2 -> \infty$ [10]. In the weak turbulence regime, the Rytov method is commonly used to represent the field of electromagnetic wave as follows [10] (using cylindrical coordinates $R = (r, L)$, with L being the transmission distance)

$$U(\boldsymbol{R}) \equiv U(\boldsymbol{r}, L) = U_0(\boldsymbol{r}, L)\ \exp[\psi(\boldsymbol{r}, L)] \tag{2}$$

where $U_0(\boldsymbol{r}, L)$ is the electromagnetic field in the absence of turbulence, and ψ is the complex phase perturbation because of turbulence. The complex phase perturbation can be expressed as follows

$$\psi(\boldsymbol{r}, L) = \log\left[\frac{U(\boldsymbol{r}, L)}{U_0(\boldsymbol{r}, L)}\right] = X + jY \tag{3}$$

where X is the log-amplitude fluctuation and Y is the corresponding phase fluctuation. In the weak turbulence regime it is reasonable to assume X and Y to be Gaussian random processes. To deal with phase fluctuations someone may use active modal compensation of wave-front phase distortion [13]. The residual phase variance after modal compensation can be described in terms of Zernike terms by [13]

$$\sigma_Y^2 = Z_J \left(\frac{D}{d_0}\right)^{5/3} \tag{4}$$

where D is the aperture diameter, d_0 is the correlation length and Z_J denotes the Jth Zenrike term not being compensated (commonly $J = 3, 6, 10, 20$). Through the paper we assume $D < d_0$ and that the Zenrike terms beyond 5 are not compensated, leading to typical σ_Y being between 0.01 and 0.1. We further assume that the OFDM system is designed such that $T_{\mathrm{OFDM}} < \tau_0$, where T_{OFDM} is the OFDM symbol duration and τ_0 is the correlation time, typically between 10 μs and 10 ms. Therefore the Gaussian process $X(t)$ can be described by multivariate Gaussian distribution

$$f_{X(t_1),\ldots,X(t_n)}(x_1, \ldots, x_n) = \frac{1}{(2\pi)^{n/2}\det(\boldsymbol{C}_X)} \times \exp\left[-\frac{1}{2}(\boldsymbol{x}-\boldsymbol{\mu})^{\mathrm{T}} \boldsymbol{C}_X^{-1}(\boldsymbol{x}-\boldsymbol{\mu})\right] \tag{5}$$

where $\boldsymbol{x} = [x_1 \ldots x_n]^{\mathrm{T}}$, $\boldsymbol{\mu} = [E\{X(t_1)\} \ldots E\{X(t_{\mathrm{n}})\}]^{\mathrm{T}}$, with $E[\cdot]$ being the expectation operator. $\boldsymbol{C}_{\mathrm{X}}$ is the covariance matrix with elements $(\boldsymbol{C}_{\mathrm{X}})_{i,j} = \sigma_X^2 b_X(|i-j| T_{\mathrm{OFDM}}/\tau_0)$, where the covariance function $b_X(\tau)$ is found to be exponential for both plane and spherical waves [10, 12]

$$b_X(\tau) = \exp\left[-\left(\frac{|\tau|}{\tau_0}\right)^{5/3}\right] \tag{6}$$

σ_X^2 denotes the variance of the log-normally distributed amplitude, which for plane wave can be approximated as [10]

$$\sigma_X^2 \cong 0.56\, k^{7/6} \int_0^L C_n^2(x)(L-x)^{5/6}\, \mathrm{d}x \tag{7}$$

where the wave number k, propagation length L and the refractive index structure parameter C_n were introduced earlier. Note that σ_X is different from Rytov standard deviation σ_{R} used earlier and for horizontal paths $\sigma_{\mathrm{R}} \simeq 2\sigma_X$. Therefore for the weak turbulence regime $\sigma_X < 0.5$.

We turn our attention now to the fibre-optic channel model. For the first-order PMD study the Jones matrix, neglecting the polarisation-dependent loss and depolarisation effects because of non-linearity, can be represented in a manner similar to [14] by

$$\boldsymbol{H}(\omega) = \begin{bmatrix} h_{xx} & h_{xy} \\ h_{yx} & h_{yy} \end{bmatrix} = \boldsymbol{R}^{-1}\boldsymbol{P}(\omega)\boldsymbol{R},\ \ \boldsymbol{P}(\omega) = \begin{bmatrix} \mathrm{e}^{-\mathrm{j}\omega\tau/2} & 0 \\ 0 & \mathrm{e}^{\mathrm{j}\omega\tau/2} \end{bmatrix} \tag{8}$$

where τ denotes DGD, $R = R(\theta, \varepsilon)$ is the rotational matrix defined by

$$\boldsymbol{R} = \begin{bmatrix} \cos\left(\frac{\theta}{2}\right)\mathrm{e}^{\mathrm{j}\varepsilon/2} & \sin\left(\frac{\theta}{2}\right)\mathrm{e}^{-\mathrm{j}\varepsilon/2} \\ -\sin\left(\frac{\theta}{2}\right)\mathrm{e}^{\mathrm{j}\varepsilon/2} & \cos\left(\frac{\theta}{2}\right)\mathrm{e}^{-\mathrm{j}\varepsilon/2} \end{bmatrix}$$

θ denotes the polar angle, ε denotes the azimuth angle and ω the angular frequency. For coherent detection OFDM, the received symbol vector $\boldsymbol{r}_{i,k} = [r_{x,i,k}\ r_{y,i,k}]^{\mathrm{T}}$ at the ith OFDM

symbol and kth subcarrier can be represented by

$$\boldsymbol{r}_{i,k} = \alpha_i(k)\mathrm{e}^{\mathrm{j}\phi_Y}\boldsymbol{H}(k)\boldsymbol{s}_{i,k}\mathrm{e}^{\mathrm{j}\phi_{CD}(k)}\mathrm{e}^{\mathrm{j}\phi_{PN}} + \boldsymbol{n}_{i,k} \quad (9)$$

where $\boldsymbol{s}_{i,k} = [s_{x,i,k}\ \ s_{y,i,k}]^{\mathrm{T}}$ denotes the transmitted symbol vector, $\boldsymbol{n}_{i,k} = [n_{x,i,k}\ n_{y,i,k}]^{\mathrm{T}}$ denotes the noise vector because of the amplified spontaneous emission (ASE) and the Jones matrix $\boldsymbol{H}$ was introduced in (8). Here we use index k to denote the kth subcarrier frequency ω_k. $\phi_{\mathrm{CD}}(k)$ denotes the phase distortion of the kth subcarrier because of chromatic dispersion. ϕ_{PN} denotes the phase noise process $\phi_{\mathrm{PN}} = \phi_{\mathrm{T}} - \phi_{\mathrm{LO}}$ because of the laser phase noise processes of transmitting laser ϕ_{T} and local laser ϕ_{LO} that are commonly modelled as the Wiener–Lévy processes [15], which are a zero-mean Gaussian processes with corresponding variances being $2\pi\Delta\nu_{\mathrm{T}}|t|$ and $2\pi\Delta\nu_{\mathrm{LO}}|t|$, where $\Delta\nu_{\mathrm{T}}$ and $\Delta\nu_{\mathrm{LO}}$ are the laser linewidths of transmitting and receiving laser, respectively. $\alpha_i(k)$ denotes the log-amplitude attenuation coefficient because of the atmospheric turbulence channel and ϕ_Y is the residual phase noise process that remained after modal-phase compensation, as described above. From (9) we can create the equivalent OFDM channel model as shown in Fig. 3.

4 Description of the receiver and transmission diversity scheme

In this section we describe the operation of the receiver by observing two different transmission scenarios. In the first scenario we assume that the transmitter does not have any knowledge about the FSO channel. In the second scenario we assume that the transmitter has knowledge about the FSO link, which is obtained by using the short training sequence transmitted towards the retro-reflector. In both scenarios we assume that the receiver knows the properties of the fibre-optic portion of the network obtained by pilot-aided channel estimation. This can be achieved by organising the OFDM symbols in OFDM packets with several initial OFDM symbols being used for channel estimation. Note that this approach is also effective in estimating the FSO channel properties in the regime of weak turbulence. The immunity to atmospheric turbulence can be improved by employing the diversity approaches [16]. To maximise the receiver diversity, the multiple receivers should be separated enough so that independency condition is satisfied. Given the fact that the laser beam is getting expanded, during propagation it might not be possible always to separate the receivers sufficiently enough so that the independence condition is satisfied. On the other hand, by using transmission diversity instead, the independence condition is easier to satisfy. Moreover, it has been shown in [17] that transmitter diversity performs better comparable to the maximum-ratio combining receiver diversity. In transmission diversity, the signal to be transmitted from the ith transmitter, characterised by path gain $r_i \exp[-\mathrm{j}\theta_i]$, is pre-multiplied by complex gain $\alpha_i = a_i \exp[-\mathrm{j}\theta_i]$ $(0 \le a_i \le 1)$. On the receiver side, the weight a_i that maximises the signal-to-noise ratio is chosen by [17]

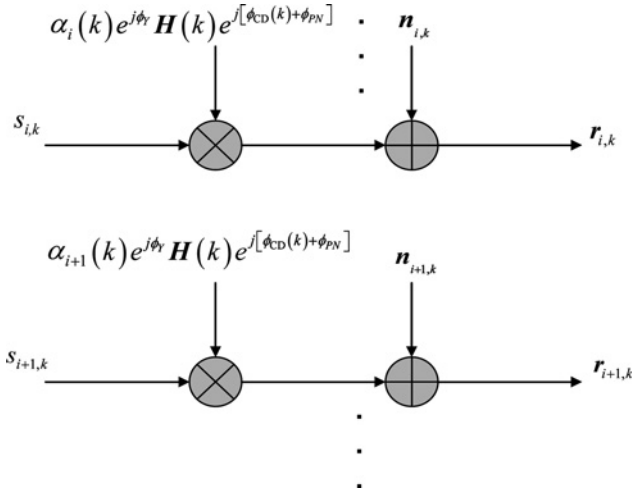

Figure 3 *Equivalent OFDM channel model for hybrid optical networks*

$$a_i = \frac{r_i}{\sqrt{\sum_{i=1}^{L} r_i^2}}$$

where L is the number of transmitter branches. When the channel is not known on the transmitter side, we have to set up a_i to 1, and $\theta_i = 0$, and use the Alamouti-type scheme instead [16, 17]. Note, however, that the Alamouti-type receiver requires the knowledge of the FSO channel, and as such is not considered here.

The operations of all blocks of receiver, except the symbol detector shown in Fig. 2*d*, are similar to those we reported in [9, 12]; for more details on OFDM with coherent detection and chromatic dispersion compensation an interested reader is referred to [4]. Here we describe the operation of the symbol detector block, the calculation of symbol log-likelihood ratios (LLRs) and the calculation of bit LLRs, in the presence of laser phase noise. By re-writing (9) in scalar form, we obtain, by ignoring the laser phase noise at the moment to keep the explanation simpler

$$r_{x,i,k} = a_i(k)\alpha_i(k)\mathrm{e}^{\mathrm{j}\phi_Y}\left[h_{xx}(k)s_{x,i,k} + h_{xy}(k)s_{y,i,k}\right] + n_{x,i,k} \quad (10)$$

$$r_{y,i,k} = a_i(k)\alpha_i(k)\mathrm{e}^{\mathrm{j}\phi_Y}\left[h_{yx}(k)s_{x,i,k} + h_{yy}(k)s_{y,i,k}\right] + n_{y,i,k} \quad (11)$$

where we used the index k to denote the kth subcarrier, index i to denote the ith OFDM symbol, $h_{ij}(k)$ $(i, j \in \{x, y\})$ are the channel coefficients because of PMD introduced by (8), $s_{x,i,k}$ and $s_{y,i,k}$ denote the transmitted symbols in x- and y-polarisation, respectively; whereas the corresponding received symbols are denoted by $r_{x,i,k}$ and $r_{y,i,k}$. The weight a_i is chosen in such a way so as to maximise the SNR, as explained above. In (10) and (11) $n_{x,i,k}$ and $n_{y,i,k}$ denote the ASE noise processes in x- and y-polarisation. In the absence of ASE noise, (10) and (11) represent the system of linear equations with two unknowns $s_{x,i,k}$ and $s_{y,i,k}$, and

doi: 10.1049/iet-opt.2008.0059

upon solving we obtain

$$\tilde{s}_{x,i,k} = \frac{h_{xx}^*/|h_{xx}|^2\left[r_{x,i,k} - h_{xy}h_{yy}^*/|h_{yy}|^2\, r_{y,i,k}\right]}{1 - \left(h_{xx}^*h_{xy}/|h_{xx}|^2\right)\left(h_{yx}h_{yy}^*/|h_{yy}|^2\right)} \tag{12}$$

$$\tilde{s}_{y,i,k} = \frac{h_{yy}^*}{|h_{yy}|^2} r_{y,i,k} - \frac{h_{yx}h_{yy}^*}{|h_{yy}|^2}\tilde{s}_{x,i,k} \tag{13}$$

where $\tilde{s}_{x,i,k}$ and $\tilde{s}_{y,i,k}$ denote the detector estimates of symbols $s_{x,i,k}$ and $s_{y,i,k}$ transmitted on the kth subcarrier of ith OFDM symbol. Note that the OFDM scheme with polarisation diversity [4], assuming that both polarisations are used on a transmitter side and equal-gain combining on a receiver side, is the special case of the symbol detector described by (12) and (13). By setting $s_{x,i,k} = s_{y,i,k} = s_{i,k}$ and using the symmetry of channel coefficients, the transmitted symbol can be estimated by

$$\tilde{s}_{i,k} = \frac{h_{xx}^* r_{x,i,k} + h_{xy}^* r_{y,i,k}}{|h_{xx}|^2 + |h_{xy}|^2}$$

In the presence of laser phase noise the symbol detector estimates are function of the laser phase noise process

$$\tilde{s}_{x,i,k} = \frac{(h_{xx}^*/|h_{xx}|^2)\mathrm{e}^{-\mathrm{j}\phi_{\mathrm{PN}}}\left[r_{x,i,k} - (h_{xy}h_{yy}^*/|h_{yy}|^2) r_{y,i,k}\right]}{1 - (h_{xx}^*h_{xy}/|h_{xx}|^2)(h_{yx}h_{yy}^*/|h_{yy}|^2)} \tag{14}$$

$$\tilde{s}_{y,i,k} = \frac{h_{yy}^*\mathrm{e}^{-\mathrm{j}\phi_{\mathrm{PN}}}}{|h_{yy}|^2} r_{y,i,k} - \frac{h_{yx}h_{yy}^*}{|h_{yy}|^2}\tilde{s}_{x,i,k} \tag{15}$$

The detector soft estimates of symbols carried by the kth subcarrier in the ith OFDM symbol, $\tilde{s}_{x(y)i,k}$, are forwarded to the a posteriori probability (APP) demapper, which determines the symbol LLRs $\lambda_{x(y)}(s)$ of x- (y-) polarisation by

$$\lambda_{x(y)}(s|\phi_{\mathrm{PN}}) = -\frac{\left(\mathrm{Re}\left[\tilde{s}_{i,k,x(y)}(\phi_{\mathrm{PN}})\right] - \mathrm{Re}[\mathrm{QAM}(\mathrm{map}(s))]\right)^2}{2\sigma^2} - \frac{\left(\mathrm{Im}\left[\tilde{s}_{i,k,x(y)}(\phi_{\mathrm{PN}})\right] - \mathrm{Im}[\mathrm{QAM}(\mathrm{map}(s))]\right)^2}{2\sigma^2}$$
$$s = 0, 1, \ldots, 2^{n_{\mathrm{b}}} - 1 \tag{16}$$

where Re[] and Im[] denote the real and imaginary parts of a complex number, QAM denotes the QAM-constellation diagram, σ^2 denotes the variance of an equivalent Gaussian noise process originating from ASE noise and map(s) denotes a corresponding mapping rule (Gray mapping rule is applied here). (n_{b} denotes the number of bits carried by a symbol.) Note that symbol LLRs in (16) are conditioned on the laser phase noise sample $\phi_{\mathrm{PN}} = \phi_{\mathrm{T}} - \phi_{\mathrm{LO}}$, which is a zero-mean Gaussian process (the Wiener–Lévy process [15]) with variance $\sigma_{\mathrm{PN}}^2 = 2\pi(\Delta\nu_{\mathrm{T}} + \Delta\nu_{\mathrm{LO}})|t|$ ($\Delta\nu_{\mathrm{T}}$ and $\Delta\nu_{\mathrm{LO}}$ are the corresponding laser linewidths introduced earlier). This comes from the fact that estimated symbols $\tilde{s}_{x(y)i,k}$ are functions of ϕ_{PN}. To remove the dependence on ϕ_{PN}, we have to average the likelihood function (not its logarithm), overall possible values of ϕ_{PN}

$$\lambda_{x(y)}(s) = \log\left\{\int_{-\infty}^{\infty} \exp\left[\lambda_{x(y)}(s|\phi_{\mathrm{PN}})\right]\frac{1}{\sigma_{\mathrm{PN}}\sqrt{2\pi}} \times \exp\left(-\frac{\phi_{\mathrm{PN}}^2}{2\sigma_{\mathrm{PN}}^2}\right)\mathrm{d}\phi_{\mathrm{PN}}\right\} \tag{17}$$

The calculation of LLRs in (17) can be performed by numerical integration. For the laser linewidths considered in this paper it is sufficient to use the trapezoidal rule, with samples of ϕ_{PN} obtained by pilot-aided channel estimation as explained in [4].

Let us denote by $b_{j,x(y)}$ the jth bit in an observed symbol s binary representation $\boldsymbol{b} = (b_1, b_2, \ldots, b_{\mathrm{nb}})$ for x- (y-) polarisation. The bit LLRs required for LDPC decoding are calculated from the symbol LLRs by

$$L(\hat{b}_{j,x(y)}) = \log\frac{\sum_{s:b_j=0}\exp\left[\lambda_{x(y)}(s)\right]}{\sum_{s:b_j=1}\exp\left[\lambda_{x(y)}(s)\right]} \tag{18}$$

Therefore the jth bit LLR in (18) is calculated as the logarithm of the ratio of a probability that $b_j = 0$ and $b_j = 1$. In the nominator, summation is performed over all symbols s having 0 at the position j. Similarly, in the denominator summation is performed over all symbols s having 1 at the position j. The bit LLRs calculated by (18) are forwarded to the corresponding LDPC decoders. The LDPC decoders from Fig. 2*d* employ the sum-product-with-correction term algorithm. The LDPC code used in this paper belong to the class of quasi-cyclic (array) codes of large girth ($g \geq 10$) [2, 18], so that the corresponding decoder complexity is low compared to random LDPC codes, and do not exhibit the error floor phenomena in the region of interest in fibre-optics communications ($\leq 10^{-15}$).

The parity check-matrix $\boldsymbol{H}$ of quasi-cyclic (QC) (N, K) LDPC codes [18] considered in this paper can be

represented by

$$\boldsymbol{H} = \begin{bmatrix} I & I & I & \dots & I \\ I & P^{S[1]} & P^{S[2]} & \dots & P^{S[c-1]} \\ I & P^{2S[1]} & P^{2S[2]} & \dots & P^{2S[c-1]} \\ \dots & \dots & \dots & \dots & \dots \\ I & P^{(r-1)S[1]} & P^{(r-1)S[2]} & \dots & P^{(r-1)S[c-1]} \end{bmatrix}$$

where $\boldsymbol{I}$ is the $p \times p$ (p is a prime number) identity matrix, P is the $p \times p$ permutation matrix ($p_{i,i+1} = p_{p,1} = 1$, $i = 1, 2, \dots, p-1$; other elements of P are zeros), whereas r and c represent the number of rows and columns, respectively. The set of integers S are to be carefully chosen from the set $\{0, 1, \dots, p-1\}$ so that the cycles of short length, in corresponding Tanner (bipartite) graph representation of the parity-check matrix, are avoided. A bipartite (Tanner) graph is a graph whose nodes may be separated into two classes (variable and check nodes), and where undirected edges may only connect two nodes not residing in the same class. The Tanner graph of a code is drawn according to the following rule: check (function) node c is connected to variable (bit) node v whenever element h_{cv} in a parity-check matrix $\boldsymbol{H}$ is a 1. There are N-K check nodes and N variable nodes. As an illustrative example, consider the $\boldsymbol{H}$-matrix of the following LDPC code

$$\boldsymbol{H} = \begin{bmatrix} 1 & 0 & 1 & 0 & 1 & 0 \\ 1 & 0 & 0 & 1 & 0 & 1 \\ 0 & 1 & 1 & 0 & 0 & 1 \\ 0 & 1 & 0 & 1 & 1 & 0 \end{bmatrix}$$

For any valid codeword $\boldsymbol{v} = [v_0\, v_1 \dots v_{N-1}]$, the checks used to decode the codeword are written as

- Equation (c_0): $v_0 + v_2 + v_4 = 0 \pmod 2$
- Equation (c_1): $v_0 + v_3 + v_5 = 0 \pmod 2$
- Equation (c_2): $v_1 + v_2 + v_5 = 0 \pmod 2$
- Equation (c_3): $v_1 + v_3 + v_4 = 0 \pmod 2$

The bipartite graph (Tanner graph) representation of this code is given in Fig. 4*a*. The circles represent the bit (variable) nodes, whereas the squares represent the check (function) nodes. For example, the variable nodes v_0, v_2 and v_4 are involved in equation (c_0), and therefore connected to the check node c_0. A closed path in a bipartite graph comprising l edges that closes back on itself is called a cycle of length l. The shortest cycle in the bipartite graph is called the girth. The girth influences the minimum distance of LDPC codes, correlates the extrinsic LLRs and therefore affecting the decoding process. The use of large girth LDPC codes is preferable because the large girth increases the minimum distance, and de-correlates the extrinsic info in the decoding process. To check for the existence of short cycles, one has to search over $\boldsymbol{H}$-matrix for the patterns shown in Figs. 4*b* and *c*. The codeword length is determined

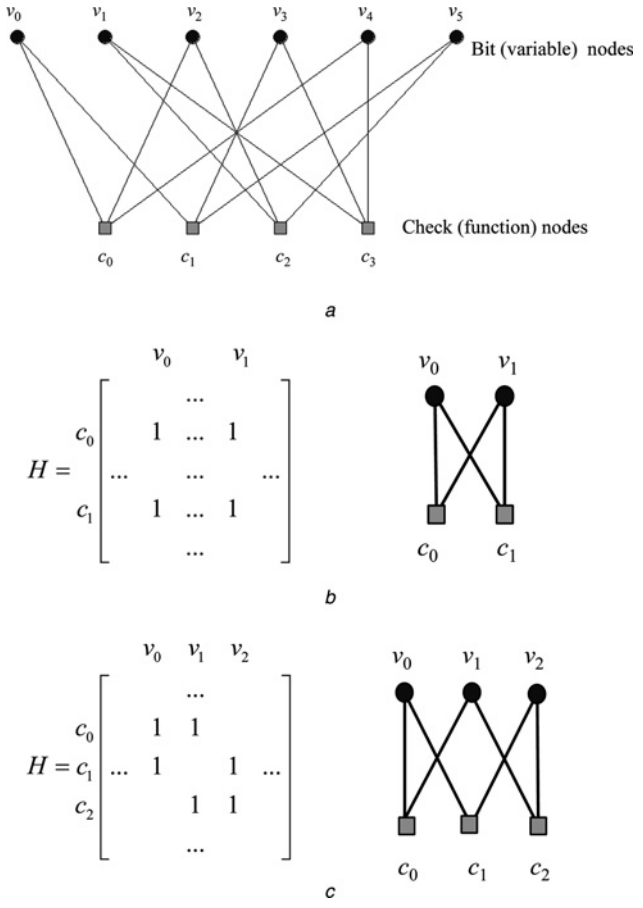

Figure 4 *Identification of short cycles in bipartite graph representation of a parity-check matrix*

a Bipartite graph of LDPC(6,2) code described by $\boldsymbol{H}$ matrix above. Cycles in a Tanner graph
b Cycle of length 4
c Cycle of length 6

by $N = |S|p$, where $|S|$ denotes the cardinality of set S, and the code rate is lower bounded by $(1\text{-}r/|S|)$. For example, by selecting $p = 1123$ and $S = \{0, 2, 5, 13, 20, 37, 58, 91, 135, 160, 220, 292, 354, 712, 830\}$ an LDPC code of rate 0.8, girth $g = 10$, column weight 3 and length $N = 16\,845$ is obtained. For more details on LDPC codes an interested reader is referred to an excellent book by MacKay [19].

5 Evaluation of the proposed hybrid optical network

We are turning our attention to the evaluation of the proposed hybrid optical network. We first compare the BER performance of the employed girth-10 LDPC codes against RS codes, concatenated RS codes, turbo-product codes (TPCs) and other classes of LDPC codes. The results of simulations for an additive white Gaussian noise (AWGN) channel model are given in Fig. 5. The girth-10 LDPC(24015,19212) code of rate 0.8 outperforms the concatenation RS(255,239) + RS(255,223) (of rate 0.82) by 3.35 dB and RS(255,239) by 4.75 dB, both at BER of 10^{-7}. The same LDPC code outperforms projective

IET Optoelectron., 2010, Vol. 4, Iss. 1, pp. 17–28
doi: 10.1049/iet-opt.2008.0059

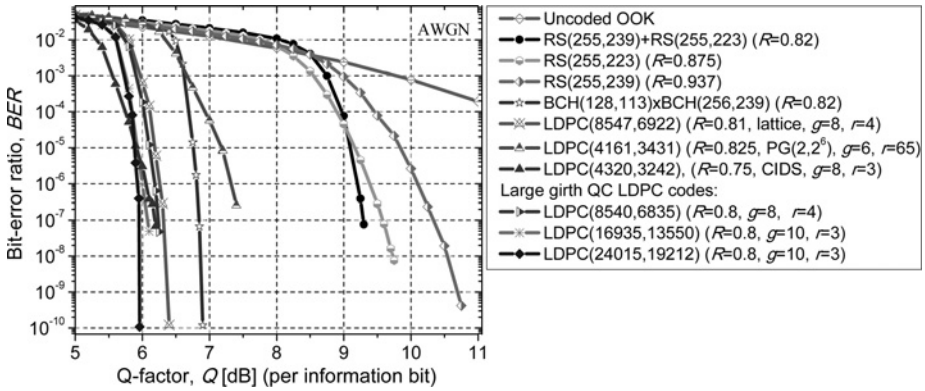

Figure 5 *Large girth QC LDPC codes against RS codes, concatenated RS codes, TPCs, and previously proposed LDPC codes*

geometry (PG) $(2,2^6)$-based LDPC(4161,3431) (of rate 0.825) of girth-6 by 1.49 dB at a BER of 10^{-7}, and outperforms girth-8 LDPC(4320,3242) of rate 0.75 by 0.25 dB. At a BER of 10^{-10} it outperforms lattice-based LDPC(8547,6922) of rate 0.81 and girth-8 by 0.44 dB, and BCH(128,113)xBCH(256,239) TPC of rate 0.82 by 0.95 dB. The net effective coding gain at aBER of 10^{-12} is 10.95 dB.

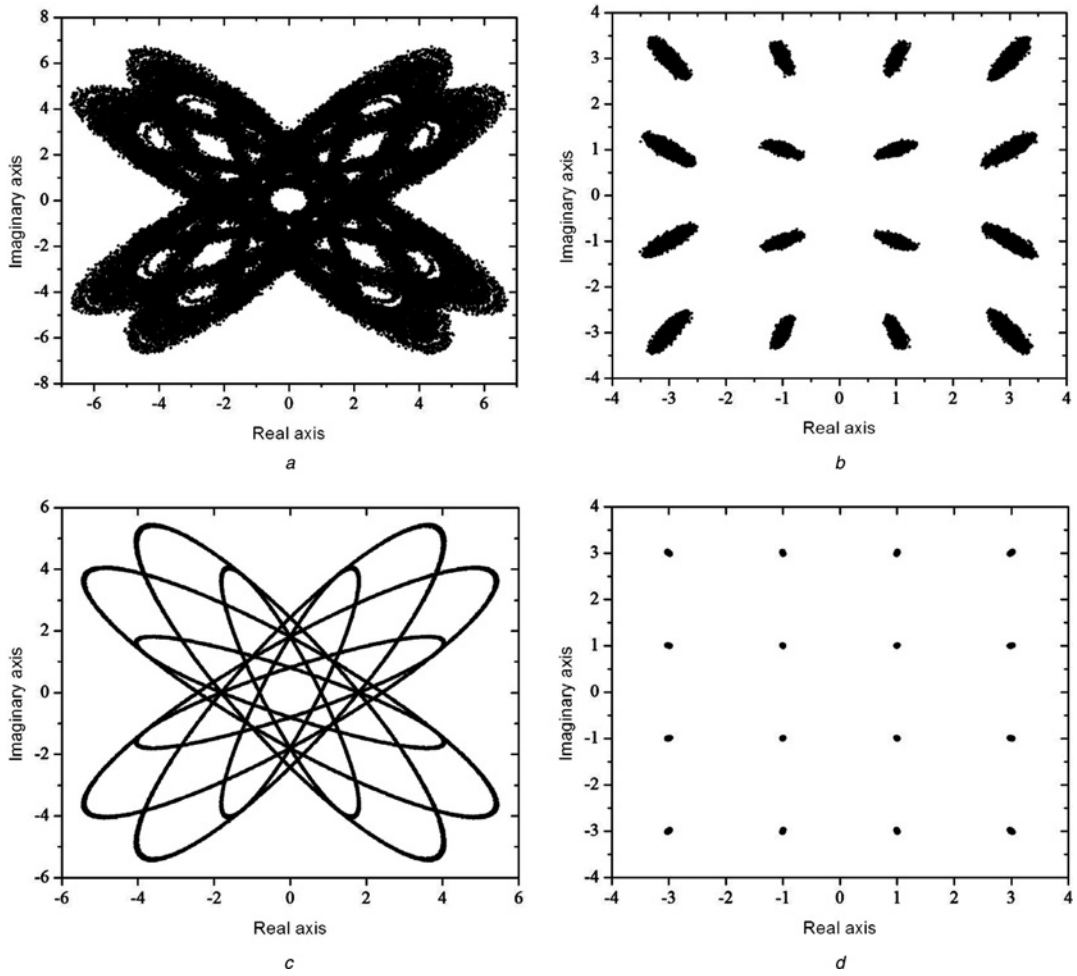

Figure 6 *The constellation diagrams for polarisation-multiplexed 16-QAM (the aggregate data rate is 100 Gb/s) after 500 ps of DGD for $\sigma_X = 0.1$, $\sigma_Y = 0.05$ and OSNR = 50 dB observing the worst case scenario ($\theta = \pi/2$ and $\varepsilon = 0$) without transmission diversity*

a Before PMD compensation
b After PMD compensation. The corresponding constellation diagrams in the presence of PMD only (for DGD of 500 ps)
c Before PMD compensation
d After PMD compensation

In the simulation results shown in Figs. 6 and 7 we assume that PMD channel coefficients are known at the receiver, because they can easily be determined by pilot-aided channel estimation [3, 4]. On the other hand, the FSO channel may change significantly during the day time, and as such is difficult to estimate. To illustrate the efficiency of this scheme, in Figs. 6*a* and *b* we show the constellation diagrams for an aggregate rate of 100 Gb/s, corresponding to the $M = 16$ QAM and the OFDM signal bandwidth of 12.5 GHz in the presence of atmospheric turbulence ($\sigma_X = 0.1$ and $\sigma_Y = 0.05$), before (see Fig. 6*a*) and after (see Fig. 6*b*) PMD compensation, assuming the worst-case scenario ($\theta = \pi/2$ and $\varepsilon = 0$). The corresponding constellation diagrams in the presence of PMD only are shown in Figs. 6*c* and *d*. The proposed coded-modulation scheme is able to compensate for the PMD with DGD of even 500 ps in the presence of atmospheric turbulence characterised by $\sigma_X = 0.1$ and $\sigma_Y = 0.01$.

In Fig. 7 we show the BER performance of the proposed scheme for both uncoded case (Fig. 7*a*) and LDPC-coded case (Fig. 7*b*). The OFDM system parameters were chosen as follows: the number of QAM symbols $N_{QAM} = 4096$, the oversampling is two times, the OFDM signal bandwidth is set to either 10 GHz ($M = 32$) or 12.5 GHz ($M = 16$) and the number of samples used in cyclic extension $N_G = 64$. For the fair comparison of different M-ary schemes the optical signal-to-noise ration (OSNR) on the x-axis is given per information bit, which is also consistent with digital communication literature [20]. The code rate influence is included in Fig. 7 so that the corresponding coding gains are net-effective coding gains. The average launch power per OFDM symbol is set to -3 dBm (and similarly as in wireless communications [20] represents the power per information symbol), and the Gray mapping rule is employed. To generate the temporally correlated samples according to (6), we used the

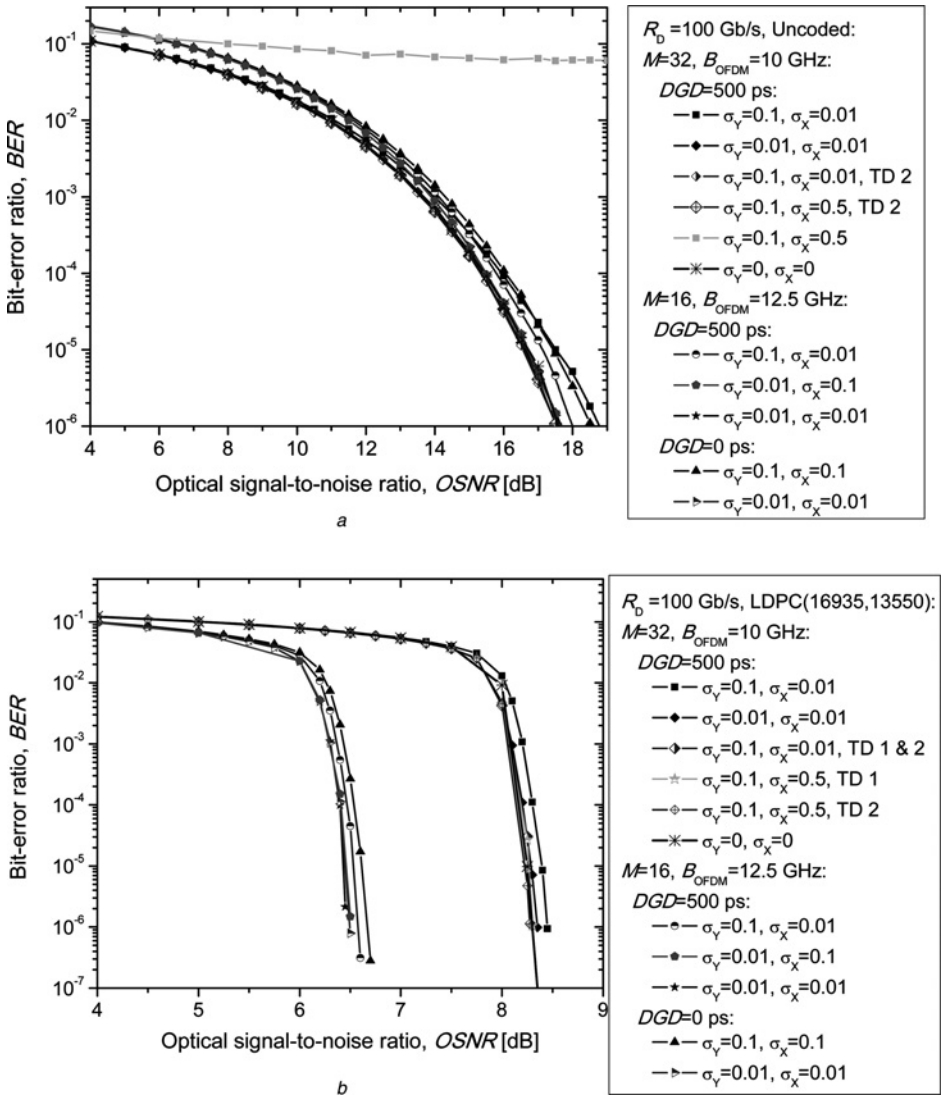

Figure 7 *BER performance of the proposed hybrid optical network scheme*

a Uncoded BER curves
b LDPC-coded BERs
R_D Denotes the aggregate data rate and B_{OFDM} is the OFDM signal bandwidth. TD *i*: transmission diversity of order *i*

IET Optoelectron., 2010, Vol. 4, Iss. 1, pp. 17–28
doi: 10.1049/iet-opt.2008.0059

Levinson–Durbin algorithm [21]. From Figs. 6 and 7 it can be concluded that PMD can be successfully compensated even in the presence of atmospheric turbulence. The most of degradation is coming from the FSO channel, as shown in Figs. 6 and 7. The 32-QAM case with aggregate data rate $R_D = 100$ Gb/s performs 1.9 dB (at BER $= 10^{-6}$) worse than 16-QAM (with the same aggregate rate) although the occupied bandwidth is smaller.

The net coded gain improvement (at BER of 10^{-6}) of LDPC-coded OFDM over uncoded OFDM is between 11.05 dB ($M = 16$, $\sigma_X = 0.01$, $\sigma_Y = 0.01$, corresponding to the weak turbulence regime) and 11.19 dB ($M = 16$, $\sigma_X = 0.1$, $\sigma_Y = 0.01$, corresponding to the medium turbulence regime). The additional coding gain improvement because of transmission diversity with two lasers is 0.19 dB for 32-QAM-based OFDM ($\sigma_X = 0.01$ and $\sigma_Y = 0.1$) at a BER of 10^{-6}. On the other hand, the improvement due to transmission diversity for the uncoded case (at the same BER) is 1.26 dB. Therefore in the regime of weak atmospheric turbulence, the improvements due to transmission diversity are moderate. On the other hand, in the moderate turbulence regime the use of transmission diversity is unavoidable. Otherwise, the uncoded BER error floor is so high (see $\sigma_X = 0.5$, $\sigma_Y = 0.1$ curve in Fig. 7*a*) that even the best LDPC codes are not able to handle, if the complexity is to be kept reasonably low. With transmission diversity, in moderate turbulence regime, we obtain BER performance comparable to the case in the absence of turbulence regime, as shown in Fig. 7. The strong turbulence regime is not considered here because of the lack of an appropriate temporal correlation model. (The atmospheric turbulence model described in Section 3 is not a valid model in the strong turbulence regime.)

The laser linewidths of transmitting and local laser were set to 10 kHz, so that the atmospheric turbulence, PMD and ASE noise are predominant effects. For the influence of laser phase noise on coherent OFDM systems, an interested reader is referred to [22]. Note that BER threshold required to achieve BER $= 10^{-6}$ at the output of the LDPC decoder is 1.96×10^{-2}, and in this region BER values for different laser linewidths are comparable.

6 Conclusion

We proposed a particular polarisation-multiplexed coded-OFDM scheme suitable for use in hybrid FSO – fibre-optics networks. This scheme is able to simultaneously deal with atmospheric turbulence, chromatic dispersion and PMD. We show that PMD can be compensated even in the presence of atmospheric turbulence. We have found that the most of the degradation comesfrom FSO channel. The proposed coded-modulation scheme supports 100 Gb/s per wavelength transmission and 100 Gb/s Ethernet. We compare the BER performance of two schemes with a fixed aggregate rate of 100 Gb/s. The first scheme employs 32-QAM and occupies 10 GHz (with a bandwidth efficiency of 10 bits/s/Hz), whereas the second scheme employs 16-QAM and occupies 12.5 GHz (with bandwidth efficiency of 8 bits/s/Hz). We have found that the 16-QAM scheme outperforms 32-QAM by 1.9 dB at a BER of 10^{-6}, although it has a higher bandwidth, because larger constellation schemes are more sensitive to the atmospheric turbulence. The net coded gain improvement (defined at a BER of 10^{-6}) of LDPC-coded 16-QAM OFDM, for $\sigma_X = 0.1$ and $\sigma_Y = 0.01$, over uncoded-OFDM 11.19 dB. The improvements because of transmission diversity are moderate in weak turbulence, and significant in moderate turbulence regime.

7 Acknowledgment

This work was supported in part by the National Science Foundation (NSF) under Grant IHCS-0725405.

8 References

[1] MINKOV L.L., DJORDJEVIC I.B., BATSHON H.G., *ET AL.*: 'Demonstration of PMD compensation by LDPC-coded turbo equalization and channel capacity loss characterization due to PMD and quantization', *IEEE Photon. Technol. Lett.*, 2007, **19**, pp. 1852–1854

[2] DJORDJEVIC I.B., MINKOV L.L., BATSHON H.G.: 'Mitigation of linear and nonlinear impairments in high-speed optical networks by using LDPC-coded turbo equalization', *IEEE J. Sel. Areas Commun.*, 2008, **26**, pp. 73–83

[3] SHIEH W., YI X., MA Y., TANG Y.: 'Theoretical and experimental study on PMD-supported transmission using polarization diversity in coherent optical OFDM systems', *Opt. Express*, 2007, **15**, pp. 9936–9947

[4] SHIEH W., YI X., MA Y., YANG Q.: 'Coherent optical OFDM: has its time come? [Invited]', *J. Opt. Netw.*, 2008, **7**, pp. 234–255

[5] ALIC N., PAPEN G.C., SAPERSTEIN R.E., *ET AL.*: 'Experimental demonstration of 10 Gb/s NRZ extended dispersion-limited reach over 600 km-SMF link without optical dispersion compensation'. Proc. OFC/NFOEC 2006, March 2006, Paper OWB7

[6] POGGIOLINI P., BOSCO G., SAVORY S., BENLACHTAR Y., KILLEY R.I., PRAT J.: '1,040 km uncompensated IMDD transmission over G.652 fiber at 10 Gbit/s using a reduced-state SQRT-metric MLSE receiver'. Proc. ECOC 2006, Cannes, France, September 2006, PDP Th4.4.6

[7] SUN H., WU K.-T., ROBERTS K.: 'Real-time measurements of a 40 Gb/s coherent system', *Opt. Express*, 2008, **16**, pp. 873–879

[8] SAVORY S.J.: 'Digital filters for coherent optical receivers', *Opt. Express*, 2008, **16**, pp. 804–817

[9] DJORDJEVIC I.B., XU L., WANG T.: 'Simultaneous chromatic dispersion and PMD compensation by using coded-OFDM and girth-10 LDPC codes', *Opt. Express*, 2008, **16**, pp. 10269–10278

[10] ANDREWS L.C., PHILIPS R.L.: 'Laser beam propagation through random media' (SPIE Press, 2005)

[11] WILLEBRAND H., GHUMAN B.S.: 'Free-space optics: enabling optical connectivity in today's networks' (Sams Publishing, 2002)

[12] DJORDJEVIC I.B., VASIC B., NEIFELD M.A.: 'LDPC coded OFDM over the atmospheric turbulence channel', *Opt. Express*, 2007, **15**, pp. 6332–6346

[13] NOLL R.J.: 'Zernike polynomials and atmospheric turbulence', *J. Opt. Soc. Am.*, 1976, **66**, pp. 207–211

[14] PENNINCKX D., MORENÁS V.: 'Jones matrix of polarization mode dispersion', *Opt. Lett.*, 1999, **24**, pp. 875–877

[15] CVIJETIC M.: 'Coherent and nonlinear lightwave communications' (Artech House, 1996)

[16] DJORDJEVIC I.B., DENIC S., ANGUITA J., VASIC B., NEIFELD M.A.: 'LDPC-coded MIMO optical communication over the atmospheric turbulence channel', *J. Lightwave Technol.*, 2008, **26**, pp. 478–487

[17] GOLDSMITH A.: 'Wireless communications' (Cambridge University Press, 2005)

[18] DJORDJEVIC I.B., XU L., WANG T., CVIJETIC M.: 'Large girth low-density parity-check codes for long-haul high-speed optical communications'. Proc. OFC/NFOEC 2008, Paper no. JWA53

[19] MACKAY D.J.C.: 'Information theory, inference, and learning algorithms' (Cambridge University Press, 2003)

[20] PROAKIS J.G.: 'Digital communications' (McGraw-Hill, 2001)

[21] DURBIN J.: 'Efficient estimation of parameters in moving-average models', *Biometrica*, 1959, **46**, pp. 306–316

[22] YI X., SHIEH W., MA Y.: 'Phase noise effects on high spectral efficiency coherent optical OFDM transmission', *J. Lightwave Technol.*, 2008, **26**, pp. 1309–1316

doi: 10.1049/iet-opt.2008.0059